Hindawi
Mathematical Problems in Engineering
Volume 2022, Article ID 1150051, 11 pages
https://doi.org/10.1155/2022/1150051

Research Article

Correction of Chinese Dance Training Movements Based on Digital Feature Recognition Technology

LinJuan Zhang

Hangzhou Normal University, Qianjiang College, HangZhou, ZheJiang 310018, China

Correspondence should be addressed to LinJuan Zhang; q0060127@hznu.edu.cn

Received 28 February 2022; Revised 22 March 2022; Accepted 4 April 2022; Published 30 April 2022

Academic Editor: Xuefeng Shao

In order to improve the effect of Chinese dance training, this paper combines digital feature recognition technology to correct and analyze Chinese dance training movements and constructs an intelligent auxiliary training system. In order to solve the travel time problem at the computationally complex interface and ensure its computational accuracy, a local adaptive triangulation technique is used in the fast-advance algorithm. Moreover, this paper designs the function of the system according to the user's needs, transforms the design concept into a figurative visual representation through the interactive prototype according to the function, carries out the visual design of the interface according to the interactive prototype, and uses the interactive technology to realize the development of the system. From the test analysis results, it can be seen that the Chinese dance training action correction system based on the digital feature recognition technology proposed in this paper has a good effect and can effectively promote the improvement of the Chinese dance training effect.

1. Introduction

As one of the important components of Chinese culture and art, Chinese classical dance has a very long and splendid development history. At present, under the general trend of carrying forward the history of the Chinese nation and advocating the inheritance of traditional Chinese cultural heritage, Chinese classical dance has received attention and has been widely disseminated and carried forward. Moreover, beautiful performances of Chinese classical dance are often seen in important celebrations and diplomatic ceremonies. In addition to performing tasks on major occasions, more tasks of Chinese classical dance are to popularize cultural and artistic performance tasks across the country and around the world and have a large number of audiences and performance participants in the folk. It is the common wish of every teacher and student engaged in this work to improve and enhance the basic training and teaching of Chinese classical dance. The teaching and scientific research work of Chinese classical dance thus carried out can not only provide urgent basic training in dance teaching but also promote the popularization of Chinese classical dance among the people, thus benefiting the majority of dance lovers in the society. Therefore, this research work has profound social significance and broad application prospects.

The existence of a digital society puts forward new requirements for dance teaching and also provides us with good development opportunities. Teachers who are responsible for dance education should face the following issues directly: (1) update dance education and teaching concepts as soon as possible, absorb new knowledge structures, broaden knowledge fields, and become learners of digital technology; (2) adapt to teachers in accordance with the shifting changes of students in the new teaching process, students are the center, and a variety of teaching methods are provided; (3) learn to apply digital tools and technologies for curriculum design and skillfully use digital tools to serve dance teaching. Digital dance teaching helps to update knowledge. With the help of a digital high-speed dissemination system and digital technology, knowledge updates will be accelerated. Various media and mobile devices provide audiences with learning conditions that are not limited by space and time, especially for students'

"fragmented" learning, which provides convenience. The ubiquitous computing and display devices, in the study of audiovisual arts, help to strengthen the interconnection of theoretical learning and practical links. Whether at school, in the dormitory, at home, or on the road, dance learning will combine theoretical knowledge with diverse practical opportunities. All in all, the constant updating of knowledge and the constant changes of new things urge us to continue to learn for a long time and adapt to the development rhythm of the digital society. As the inner force of dance teaching reform, teachers should take on the conscious of digital teaching reform and regard digital dance teaching as an important development opportunity.

This paper combines the digital feature recognition technology to carry out the correction and analysis of Chinese dance training movements and constructs an intelligent auxiliary training system to improve the correction effect of Chinese dance training movements.

2. Related Work

Today, with the explosive growth of multimedia data, various forms of multimedia information such as text, images, voice, and video are rapidly expanding. Multimedia information has become an urgent desire of people [1]. In multimedia information, video data have the most complex structure and richest information, but, due to the lack of expression means, it is also the most difficult to store, organize, and retrieve. How to effectively solve the problem of video data organization and retrieval has also become a research hotspot [2]. Traditional video retrieval methods rely on human memory to recall video content and then describe it in words. This method is often subjective and slow and has a high error rate [3]. The content-based image query and video retrieval method proposed in [4] has made a breakthrough in the research in this field. This method only needs to analyze the sequence structure of the video and distinguish the changes of the video according to the change degree of the content of the frame. Video retrieval requires finding the desired video clips in a large amount of video data, but because of the large and complex video content, video retrieval is very difficult, which is largely different from image retrieval [5]. Video is currently the most informative data, so the retrieval of video has become a prominent problem in real life. In the past ten years, after people's unremitting efforts, content-based video retrieval technology has been continuously developed and achieved exciting results [6]. The expression of video content can be divided into three levels: raw data (awdata), low-level visual content (low!evelvisualeontent), and semantic content (semanti eontent). The original data are composed of basic video units, data format, frame frequency (framearet), etc.; the low-level visual content is composed of visual features such as color, shape, and texture; the semantic content includes high-level concepts such as object (object)t, event (veen)t. [7]. In the field of video retrieval, most of the work is still in the use of low-level visual content, and the retrieval of semantic level is only carried out in specific fields [8]. Reference [9] proposes a method for automatic video annotation using human behavior analysis and domain-specific knowledge of specialized tennis matches. At the semantic level, the support of a knowledge base is generally required. Because of its complexity, progress has not been satisfactory. Video analysis is carried out on the basis of image analysis, so the visual features of images such as color, shape, and texture are naturally introduced into the video and have been widely used. In addition, in order to better express the video and solve the unsatisfactory video analysis results caused by the discontinuity of the visual features of the video in the spatiotemporal expression, people have introduced features that can reflect the continuity of the video, such as motion features (including objectmotion and canreramotion), or comprehensively use the correlation of different media, such as the recognition of sound and text in the video to assist the semantic recognition of the video [10]. Because visual features are intuitive, simple, and effective, they have been widely used in video retrieval. Even in today's increasingly in-depth research, using video's color, texture, shape, motion, and other low-level visual features to retrieve videos is still difficult and is the main method for video retrieval [11]. Video retrieval combined with traditional database technology can easily store and manage massive video data; combined with traditional Web search engine technology, it can be used to retrieve rich video information in HTML pages. In the foreseeable future, content-based video retrieval technology will be widely used in the following fields: multimedia database, intellectual property protection, digital library, network multimedia search engine, interactive television, art collection and museum management, telemedicine and military command system, etc. [12]. Although content-based video retrieval has received extensive attention and some applications, its real application is still in its infancy. At present, the main retrieval goals of video retrieval are retrieving similar videos, locating similar video segments in a video, and retrieving similar shots. [13]. Based on the characteristics of dance video, the composition and characteristics of digital video, video analysis, scene switching detection, and key frame selection are analyzed. A variety of methods are used, and on this basis, the content-by-content retrieval of video data is analyzed [14].

Dance is an art of human movement, which is human movement transformed into dance. The general human movement has the characteristics of nonstop flow and change and exists in a certain time and space while dance generally needs to be accompanied by music, wear specific costumes, and some have various props. On the other hand, there are also lighting and scenery, so dance is a spatial, temporal, and comprehensive dynamic plastic art [15]. Human movements are the activities of the whole body or part of the body, which are used to express the needs of emotion, thought, and life. According to the role of aesthetics, human body movements can be divided into two types: daily life movements and artistic movements. The former refers to various movements in ordinary life, and the latter refers to the movements that have been processed, organized, refined, and beautified, generally referring to dance movements [16]. Therefore, dance movements are

derived from the movements of the natural form of the human body and must be refined, added, and beautified artistically. From the movement of the human body's natural form to dance movement, it must be processed and developed in two aspects: one is to go through regular development, and the other is to go through purposeful development. Regular development refers to organizing Bai Ranyouxu's life movements into orderly movements, making life movements rhythmic; purposeful development means that each dance movement has a clear motive and expresses certain characteristics. These emotions and thoughts reflect the bamboo play and the strength of the dance [17]. The movement of the dance is to move and fit together. Any dance must move, but it cannot be a dance if it does not move. The dance moves are dynamic. From the perspective of form, the movements of the human body can be divided into three categories, namely shape, quality, and potential. Shape: there are size, square, height, length, straight, straight, and oblique; quality: there are rigid and soft, thickness, strength, and severity; momentum: there are rapidity, movement, gathering and dispersing, advancing and retreating, and sinking and rising. These opposing factors are properly unified in dance art, forming a harmonious dance beauty [18].

3. Digital Feature Technology Algorithm

The definition of the B-spline function is that for a given $n+1$ control point $P_i\,(i = 0, 1, \ldots n)$, the following p-th degree B-spline function is defined:

$$C_p(u) = \sum_{i=0}^{n} N_{i,p}(u) P_i, \tag{1}$$

where $N_{i,p}(u)$ is the p-order B-spline basis function, and $u = [u_0, u_i, \ldots, u_n]$ is the nondecreasing node vector set. In this paper, $P_i\,(i = 0, 1, \ldots, n)$ is connected in sequence with polyline segments to form a polygon, which is called a B-spline control polygon.

Then, the basis function of a B-spline of degree p can be defined as follows:

$$\begin{cases} N_{i,0(u)} = \begin{cases} 1, u \in [u_i, u_{i+1}), \\ 0, \text{other}, \end{cases} \\ N_{i,p(u)} = \dfrac{u - u_i}{u_{i+p} - u} N_{i,p-1(u)} + \dfrac{u_{i+p+1} - u}{u_{i+p+1} - u_{i+1}} N_{i+1,p-1(u)}, p \geq 2, \\ \text{regulations} \dfrac{0}{0} = 0. \end{cases} \tag{2}$$

Then, the B-spline basis function $N_{i,0(u)}$ of degree 0 is a step function, which is 0 everywhere outside the half-open interval $[u_i, u_{i+1})$.

From the definition of the basis function in formula (2), it can be obtained that adjusting the node vector of the B-spline function will cause the change of the curve shape, and how to calculate the node vector will directly determine its value effect. According to formula (2) and the two zero-order B-spline basis functions $N_{i,0(u)}$ and $N_{i+1,0(u)}$, then, this paper combines the two linearly to obtain the first-order B-spline basis function, and its expression is

$$\begin{aligned} N_{i,1(u)} &= \frac{u - u_i}{u_{i+1} - u_i} N_{i,0(u)} + \frac{u_{i+2} - u}{u_{i+2} - u_{i+1}} N_{i+1,0(u)} \\ &= \begin{cases} \dfrac{u - u_i}{u_{i+1} - u}, & u \in [u_i, u_{i+1}], \\ \dfrac{u_{i+2} - u}{u_{i+2} - u_{i+1}}, & u \in [u_{i+1}, u_{i+2}], \\ 0, & \text{other}. \end{cases} \end{aligned} \tag{3}$$

The subscript i of $N_{i,1(u)}$ in formula (3) is replaced by $i+1$, and the expression of $N_{i+1,1(u)}$ can be obtained, as follows:

$$= \begin{cases} \dfrac{u - u_{i+1}}{u_{i+2} - u_{i+1}}, & u \in [u_{i+1}, u_{i+2}], \\ \dfrac{u_{i+3} - u}{u_{i+3} - u_{i+2}}, & u \in [u_{i+2}, u_{i+3}], \\ 0, & \text{other}. \end{cases} \tag{4}$$

Formulas (2) and (4) can express the basis function of the quadratic B-spline as follows:

$$\begin{aligned} N_{i,2(u)} &= \frac{u - u_i}{u_{i+2} - u_i} N_{i,0(u)} + \frac{u_{i+3} - u}{u_{i+3} - u_{i+1}} N_{i+1,1(u)} \\ &= \begin{cases} \dfrac{(u - u_i)^2}{(u_{i+1} - u_i)(u_{i+2} - u_i)}, u \in [u_i, u_{i+1}], \\ \dfrac{(u - u_i)(u_{i+2} - u)}{(u_{i+2} - u_i)(u_{i+2} - u_{i+1})} + \dfrac{(u - u_{i+1})(u_{i+3} - u)}{(u_{i+3} - u_{i+1})(u_{i+2} - u_{i+1})}, u \in [u_{i+1}, u_{i+2}], \\ \dfrac{(u_{i+3} - u)^2}{(u_{i+3} - u_{i+2})(u_{i+3} - u_{i+1})}, u \in [u_{i+2}, u_{i+3}]. \end{cases} \end{aligned} \tag{5}$$

Similarly, other quadratic B-spline basis functions can be obtained by "translation" of the subscript i. P-th degree B-spline functions can be derived through the above transformation and equation (2). I will not go into details here. At the same time, the function value on each node can also be obtained according to the basis function derived above.

The cubic B-spline value used in the fast-forwarding algorithm introduced in this paper uses the uniform cubic B-spline value after the "translation" of the basis function. For example, the node vector u in the interval [0,1] can obtain the function value of the function in the interval [-3,-2],[-2,-1],[-1,0], and the process is deduced as follows.

If we assume $u_i = i\,(i = L, -1, 0, 1, L)$, after bringing the node vector u into formula (2), according to the "translation" property of the uniform B-spline basis function, we have

$$N_{0,1(u)} = \begin{cases} u, u \in [0,1), \\ 2-u, u \in [1,2), \\ 0, \text{other}, \end{cases}$$

$$N_{i,1(u)} = N_{0,1(u-i)}, i = L, -1, 0, 1, L,$$

$$N_{0,2(u)} = \begin{cases} \frac{1}{2}u^2, u \in [0,1), \\ \frac{1}{2}\left(-3+6u-2u^2\right), u \in [1,2), \\ \frac{1}{2}(3-u)^2, u \in [2,3), \\ 0, \text{other}, \end{cases} \tag{6}$$

$$N_{i,2(u)} = N_{0,2(u-i)}, i = L, -1, 0, 1, L,$$

$$N_{0,2(u)} = \begin{cases} \frac{1}{6}u^3, u \in [0,1), \\ \frac{1}{6}\left(4-12u+12u^2-3u^3\right), u \in [1,2), \\ \frac{1}{6}\left(-44+60u-24u^2+3u^3\right), u \in [2,3), \\ \frac{1}{6}(4-u)^3, u \in [3,4), \\ 0, \text{other}, \end{cases}$$

$$N_{i,3(u)} = N_{0,2(u-i)}, i = L, -1, 0, 1, L.$$

Considering the basis function of a uniform B-spline in the interval [0, 1], the nonzero polynomial function in other intervals can be calculated in the interval [0, 1], and its expression is as follows:

$$\begin{cases} N_{-1,1(u)} = 1-u, \\ N_{0,1(u)} = u, \end{cases} \quad u \in [0,1], \tag{7}$$

$$\begin{cases} N_{-2,2(u)} = \frac{1}{2}(1-u)^2, \\ N_{-2,2(u)} = \frac{1}{2}(1-u)^2, \\ N_{-2,2(u)} = \frac{1}{2}(1-u)^2, \\ N_{-1,2(u)} = \frac{1}{2}\left(1+2u-2u^2\right), u \in [0,1], \\ N_{0,2(u)} = \frac{1}{2}u^2, \end{cases} \tag{8}$$

$$\begin{cases} N_{-3,3(u)} = \frac{1}{6}(1-u)^3, \\ N_{-2,3(u)} = \frac{1}{6}\left(4-6u^2+3u^3\right), \\ N_{-1,3(u)} = \frac{1}{6}\left(1+3u+3u^2-3u^3\right), \\ N_{0,3(u)} = \frac{1}{6}u^3. \end{cases} \tag{9}$$

Equation (9) used in this papershowsthe B-spline interpolation calculation formula.

Because the digital light field is in a nonuniform layered medium, the interface changes with the depth and the regular grid nodes cannot describe the velocity nodes on the interface in detail, so the accuracy of the algorithm cannot be guaranteed. To this end, in order to calculate the travel time problem at complex interfaces and at the same time ensure its calculation accuracy, the fast forward algorithm adopts a local adaptive triangulation technique. The detailed schematic diagram of its principle is shown in Figure 1. In the study area, the adaptive triangular mesh is locally used to stitch the mesh nodes near the interface; that is, the triangulation algorithm is used to calculate and update the node travel time in the local study area, while the regular grid algorithm is still used for the grid nodes in other areas. Figure 2 shows an enlarged schematic diagram to demonstrate the technique. This detail characterization algorithm, which is only used in a specific area, can effectively save computing costs, improve efficiency, and ensure the accuracy of the fast-advance algorithm in ray-tracing calculations.

The following will describe in detail how the technology uses the triangular mesh to calculate the travel time value of the nodes on the interface. Figure 3 shows a schematic diagram of the triangular grid computing node travel time.

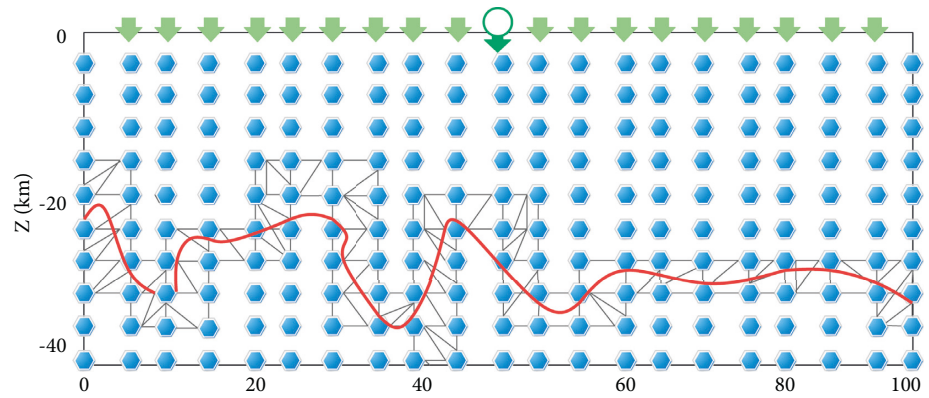

Figure 1: Schematic diagram of interface adaptive triangulation mesh.

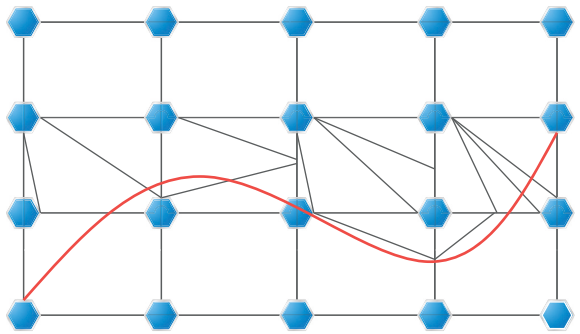

Figure 2: Schematic diagram of the enlarged view of the triangular mesh of the interface.

We assume that the travel-time values T_A and T_B of the fixed points A and B are known, and the first-order difference operator is used to solve the program function equation, and the travel-time value T_O at the point O can be obtained. If the travel time from T_A to T_O is t and $T_B > T_A$, the following quadratic equation can be obtained:

$$\begin{aligned}&\left(a^2+b^2-2ab\right)t^2+2u\left(a\cdot b-b^2\right)t\\&\quad+\left(b^2u^2-s_o^2\left[a^2b^2-\left(a^2b^2-(a\cdot b)^2\right)\right]\right)=0,\end{aligned}\tag{10}$$

where S_o is the slowness of point O, $u = T_B - T_A$, a and b are distance vectors, and $a = |a|, b = |b|$. In order to satisfy the propagation law of seismic waves, the viscous solution of formula (10) is solved, as shown in Figure 3(b). The direction of ∇T_O must be between points A and B and $u < t$; that is, it satisfies the following formula:

$$\frac{a\cdot b}{b}<\frac{b(t-u)}{t}\Bigg)<\frac{a^2b}{a\cdot b}.\tag{11}$$

Equation (10) is calculated under the condition that equation (11) is satisfied, and the travel time value at point O is obtained as $T_O = t + T_A$; in addition, $T_O = \min\{bs_o + T_A, as_o + T_B\}$, and the smaller value of the two is selected to locate the travel time of point O in area 4. As shown in Figure 3(a), in order to update the travel time at point O, it is necessary to calculate the travel time of point O of the four triangular mesh regions, respectively; that is, the same operation as above is used to obtain the travel time of point O corresponding to the triangular mesh regions 1, 2, and 3, and finally, the travel time with the smallest value and greater than zero among these four values is selected as the actual travel time value of the final point O.

It should be pointed out here that when calculating the travel time at point O, the triangular mesh must be an acute triangle. When encountering obtuse-angle triangular meshes, this calculation process does not hold, and the problem will be explained in detail below, and a reasonable explanation will be given. In order to calculate the travel time at point O, Figure 4 shows three situations that will be faced during the calculation, and in these three cases, the wavefront must propagate in the direction of point O.

(1) The triangular meshes in Figure 4(a) are all acute angles. The angles of the five nodes that diverge from the center to the point O are all 72°; that is, no matter from which angle the wavefront propagates to the point O, it will inevitably pass through two adjacent points, so the travel time at point O can be directly calculated by equation (11).

(2) The triangular meshes in Figure 4(b) are all right-angled triangles. The angles of the four nodes radiating from the center to the point O are all right angles. When the wavefront propagates to the point O, only in the four vertical directions, other angles are the same as in the first case. Figure 4(b) just shows the special case where the wavefront is incident from point A at a normal angle. Therefore, the travel time at point O in this case can be calculated by $T_O = T_A + S_O AO$.

(3) The triangular meshes in Figure 4(c) are all pin-angled triangles. Point O is the center, and the angles of the three nodes radiating from the center are all 120°. Here, the author only takes the obtuse triangle A O B as an example.

When the wavefront propagates to the point O, within the θ angle, that is, in the area of the dashed lines that are perpendicular to each other, the wavefront passes through

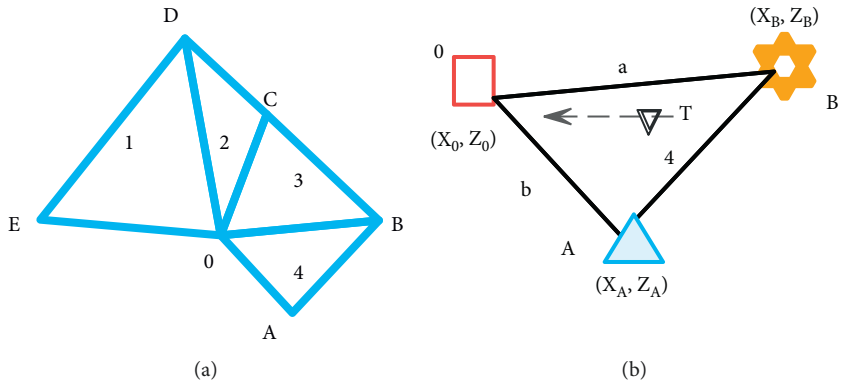

Figure 3: Schematic diagram of updating travel time in the triangle area.

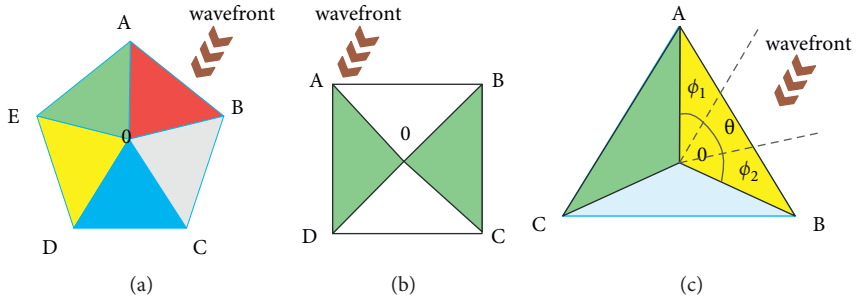

Figure 4: (a) Incident wavefront of acute triangle mesh. (b) Incident wavefront of right triangle mesh. (c) Incident wavefront of obtuse triangle mesh.

the point A and the point B. In other areas, the wavefront only passes through the point A or the point B. If the obtuse angle in Figure 4(c) is encountered, the travel time at point O is approximately calculated by $T_O = T_A + S_O AO$, and its proportion to the first-order accuracy can be specifically expressed by the following formula:

$$r = 100\left(\frac{2\psi - \pi}{\psi}\right), \tag{12}$$

where ψ is $\angle AOB$, and its size range is $\pi/2 \le \psi \le \pi$.

After the above analysis, it can be concluded that when the triangulation is obtuse angle, the calculation of the interface travel time is lower than the first-order accuracy, and the travel time calculation does not hold when encountering an obtuse triangle. However, in the actual algorithm division, the needle-angle triangle is an unavoidable problem. Therefore, Figure 5 shows a split coping strategy that is different from the previous division when facing obtuse triangles. As shown in Figure 5, (b) O is replaced by A C, and the obtuse triangle problem can be transformed into the above two situations that can be dealt with.

In this paper, a new mesh refinement strategy is adopted, which also takes into account the accuracy and computational efficiency and successfully reduces the error near the source point. Figure 6 shows the whole process of mesh refinement near the source point of the algorithm, that is, using the double mesh technique. Among them, the red solid

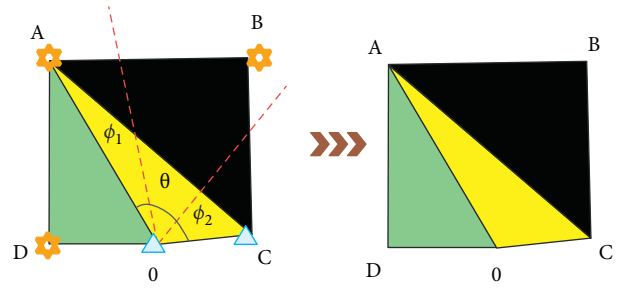

Figure 5: Alternative splitting strategy for obtuse triangles.

point is the source point, the black thick line is the narrow band, and a finer grid is used around the source point. These meshes help to characterize the narrowband in finer detail, allowing it to approximate the expansion of the simulated wavefront in a finer manner. Subsequently, the narrow band continued to expand around. When the narrow band is about to reach the boundary of the fine mesh, the mesh in this area will be instantly changed from the fine mesh to the coarse mesh. Under the premise that the computational time cost increases by an extremely small order, this refinement operation can greatly improve the computational accuracy of the fast-advance algorithm.

A heap is a completely binary tree-shaped data structure; that is, it is a sequence $\{a_1, a_2, \Lambda, a_n\}$ composed of n elements, where the elements need to satisfy $a_i \le a_{2i}, a_i \le a_{2i+1}$

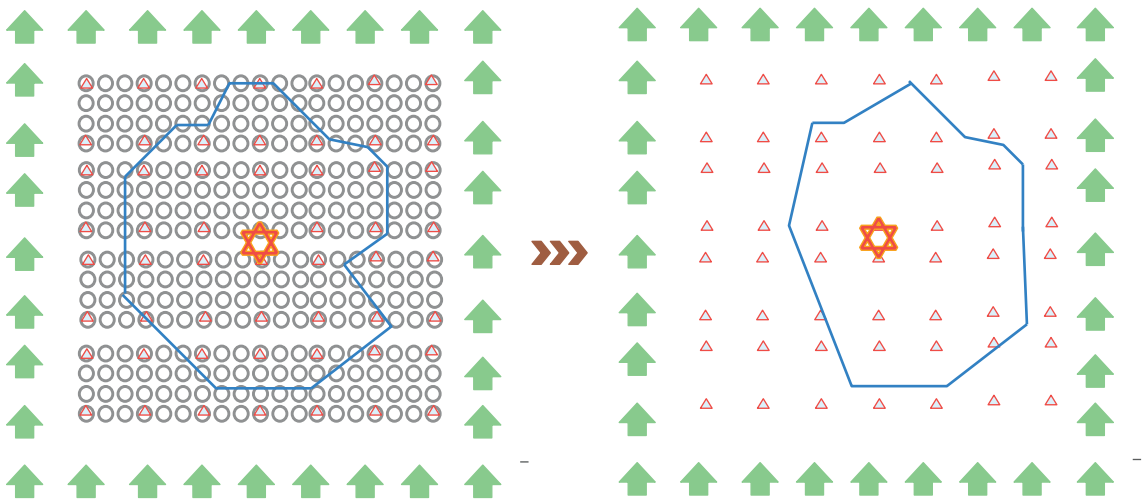

Figure 6: Mesh refinement implementation process near the source.

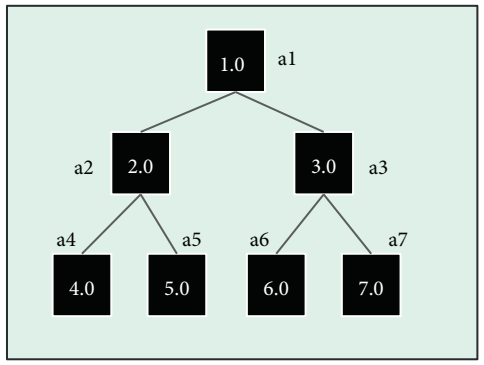

a1	a2	a3	a4	a5	a6	a7
1.0	2.0	3.0	4.0	5.0	6.0	7.0

Figure 7: The correspondence between the complete binary tree heap and each element.

or $a_i \geq a_{2i}, a_i \geq a_{2i+1}$, $(i = 1, 2, 3\Lambda, n/2)$. Then, the sequence is called a heap. The top node of the heap is called the root node. However, as a binary tree structure, each parent node has two corresponding child nodes. The minimum heap is used in the fast forward algorithm; that is, in the binary tree heap structure, the value of each parent node is smaller than its corresponding two child nodes. In a complete binary tree heap, the corresponding relationship between its data structure and its elements is shown in Figure 7. The traditional heap sorting operation process for data structure sorting includes two aspects: one is to initialize the heap, and the other is to rebuild the heap. The time complexity of its algorithm operation is $T(n) = 2n \log_2 n + o(n)$, and the size of the complexity depends on the number of comparisons between elements in the process of heap reconstruction.

We assume that there are n nodes in the narrowband at a certain moment in the process of calculating the travel time of the fast forward algorithm, and the corresponding minimum heap has n elements, and then, the structure depth of the heap is $h = [\log_2 n] + 1$. When the narrowband is expanded again, it corresponds to the operations of heap initialization and heap reconstruction. The process of performing this operation in a conventional heap is shown in Figure 8(a), which can be roughly divided into the following three steps:

(1) The algorithm removes the root element and moves the last element at the bottom of the heap to the top of the heap

(2) The algorithm takes the new root element as the parent node, compares it with the smallest child node in turn, and adjusts it downward in turn to complete the heap reconstruction

(3) The algorithm puts the newly added element into the position of the last element at the bottom of the heap, and compares and adjusts the position upward in sequence, and stops the above operations when the new minimum heap data structure is completed.

When the operations of the above three steps are continuously performed, the maximum number of comparisons between the root element and the data under the heap is $2(h-1)$. However, when the last element at the bottom of the heap is compared and adjusted upward, the maximum number of comparisons is $(h-1)$. In the process of rebuilding the heap, the maximum number of comparisons of conventional heap sorting is $3h$, and the time complexity of its algorithm is $T_1(n) = 3[\log_2 n]$. Figure 8 shows the heap operation flow of deleting 1 and adding 8.

Through the above implementation process of traditional heap sorting and combining the characteristics of narrowband expansion, it is possible to try to improve the conventional heap sorting technology. Te improved heap sorting adopts the vacancy sinking method. Compared with the traditional method, the improved heap sorting using the vacancy sinking method mainly improves the details of its contrast adjustment for the newly added elements. The improved heap sort operation can be divided into the following two steps:

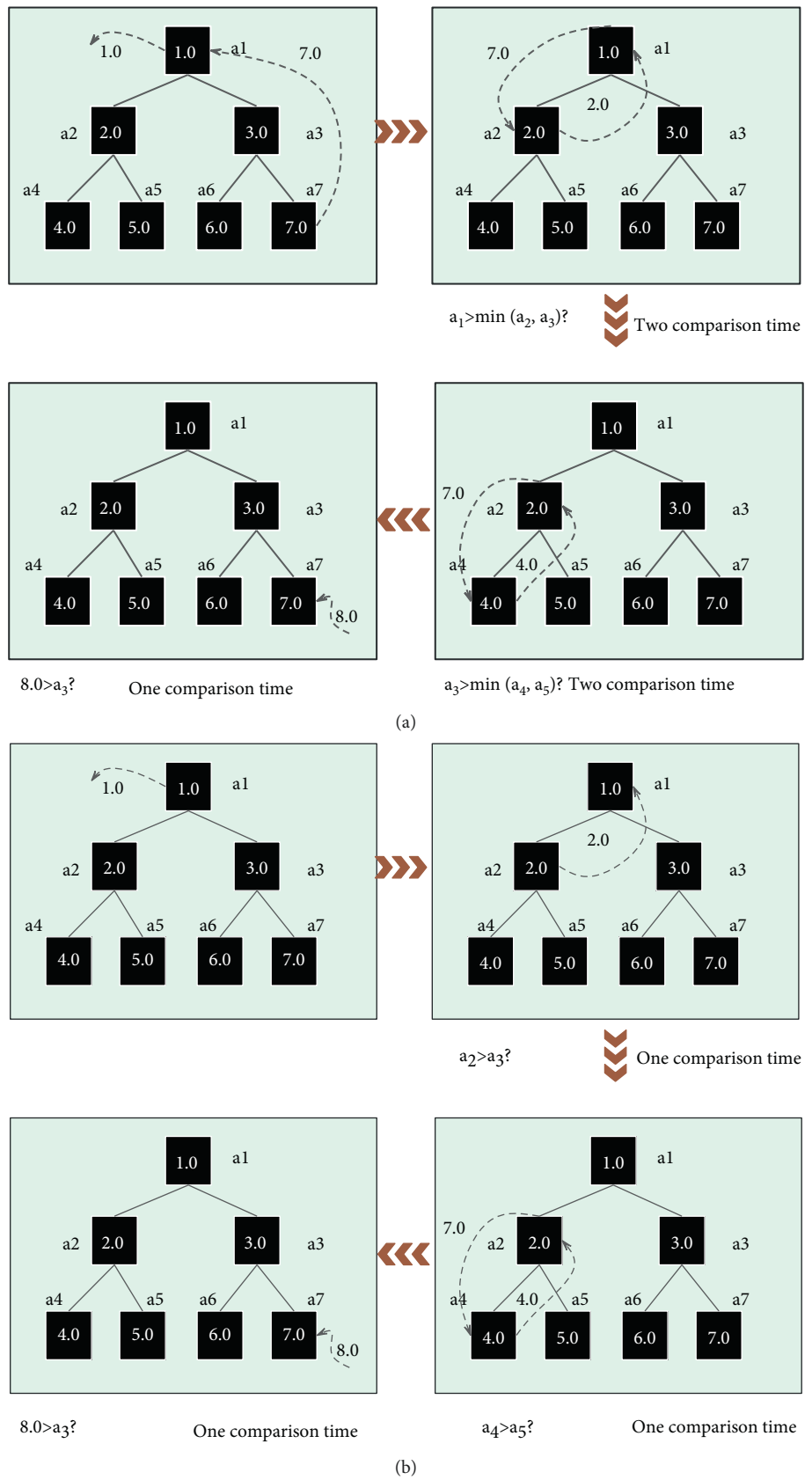

Figure 8: Flowchart of normal and improved heap sort rebuilding heap operations. (a) Regular heap sort. (b) Improve heap sort.

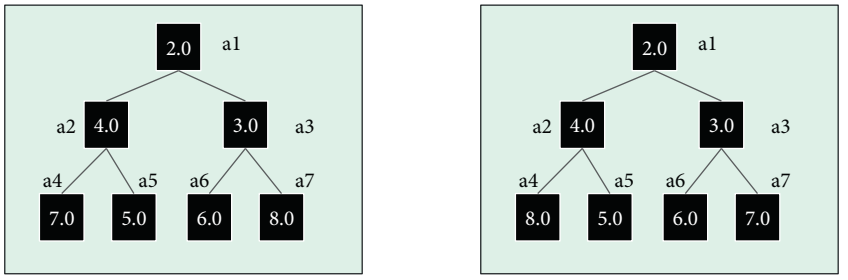

a1	a2	a3	a4	a5	a6	a7
1.0	4.0	3.0	7.0	5.0	6.0	8.0

a1	a2	a3	a4	a5	a6	a7
1.0	4.0	3.0	8.0	5.0	6.0	7.0

Figure 9: Data structure after regular and improved heap reconstruction.

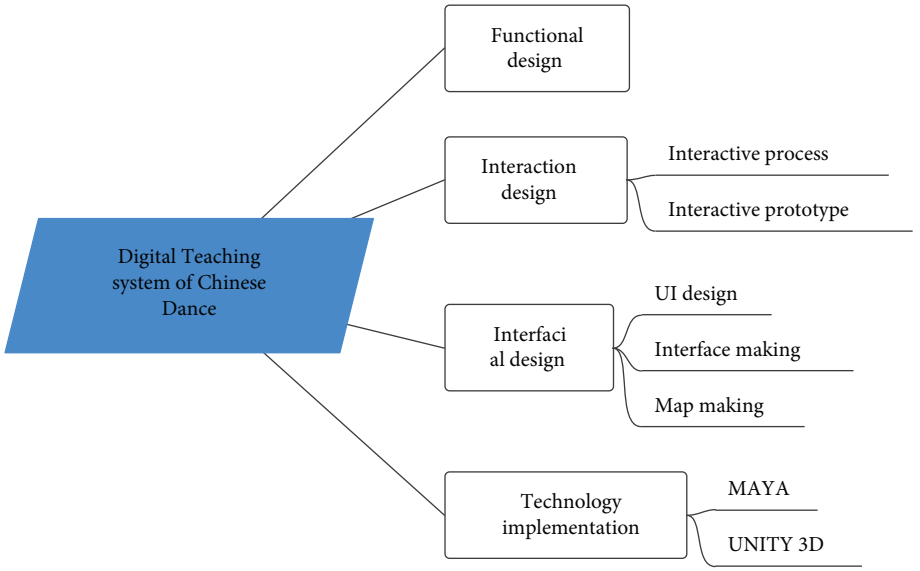

Figure 10: Correction model of Chinese dance training movements based on digital feature recognition technology.

(1) After removing the root element, its corresponding heap headspace bit is compared with its two child node values. Then, the algorithm selects the smaller of the two and swaps positions with the vacancy, and the new vacancy continues to perform the above operations on its corresponding two child nodes until the vacancy reaches the bottom layer of the heap and stops the above operations.

(2) The algorithm adds new elements to the vacancies and performs reverse and upward comparison operations according to step (1) to finally form a minimum heap data structure.

In the above process, the corresponding values of two child nodes need to be compared each time when the gap is adjusted downward, and the maximum number of comparisons is (h-1). Compared with the conventional heap sorting method, the new element inserted into the vacancy needs to be compared with its parent node each time when it is adjusted upward, and the number of comparisons is (h-1). The maximum number of comparisons for the above improved heap operation is 2(h-1), and the time complexity of the algorithm is $T_2(n) = 2[\log_2 n]$. However, according to the characteristics of the fast forward algorithm to calculate the travel time, that is, the travel time of the newly added narrowband point is always not less than the travel time corresponding to the accepting point and the original narrowband point extending this point. Therefore, considering only one comparison with its parent node when a new element is added to the vacancy, the time complexity of the conventional and improved heap sorting algorithm is $T_1(n) = 2[\log_2 n] + 1, T_2(n) = [\log_2 n] + 1$, respectively. Figure 9 shows the data structure after regular and improved heap reconstruction.

From the analysis of Figure 8 and Figure 9, in the process of rebuilding the heap, the improved heap still maintains the structure of the minimum heap although the elements corresponding to the nodes in the heap have changed. This fully demonstrates the effectiveness of this improvement for heap sort. At the same time, the improved heap is twice as efficient as the traditional conventional heap sort in terms of its numerical comparison efficiency.

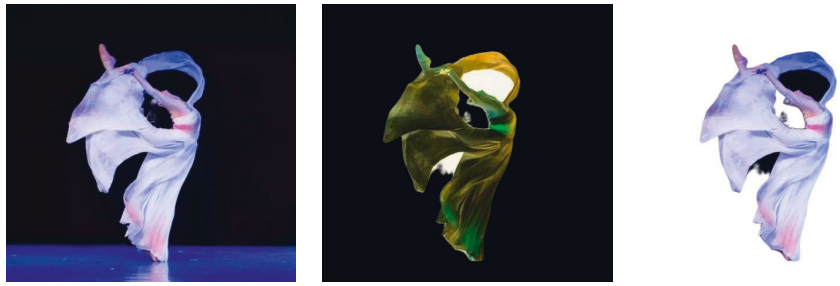

(a) (b) (c)

Figure 11: Demonstration of Chinese dance movement correction image based on digital feature recognition technology. (a) Original Chinese dance movement image. (b) Background removal of Chinese dance movement image. (c) Feature extraction of Chinese dance movement image.

Table 1: The effect of the correction system of Chinese dance training movements based on digital feature recognition technology.

VB	Training effect	Number	Training effect	Number	Training effect	Number	Training effect
1	87.20	21	86.73	41	80.31	61	83.85
2	86.99	22	78.57	42	83.15	62	88.70
3	85.57	23	79.37	43	87.75	63	80.52
4	80.26	24	89.58	44	86.18	64	82.59
5	80.92	25	89.97	45	78.58	65	82.06
6	78.27	26	81.64	46	80.38	66	83.84
7	84.40	27	84.93	47	84.90	67	85.22
8	81.15	28	81.47	48	80.97	68	85.60
9	85.40	29	90.50	49	90.37	69	83.71
10	81.73	30	87.20	50	86.86	70	84.63
11	88.11	31	83.42	51	80.31	71	86.61
12	79.53	32	87.08	52	87.77	72	78.64
13	89.62	33	85.42	53	81.07	73	82.65
14	80.97	34	80.71	54	86.23	74	78.62
15	82.40	35	86.95	55	82.62	75	88.94
16	89.73	36	89.72	56	84.86	76	88.61
17	81.13	37	84.17	57	90.83	77	80.98
18	80.32	38	90.00	58	87.99	78	86.79
19	83.09	39	79.05	59	85.96	79	86.34
20	90.82	40	80.68	60	79.79	80	90.45

4. Correction of Chinese Dance Training Movements Based on Digital Feature Recognition Technology

The design of the digital teaching system of Chinese classical dance is to design the function of the system according to the user's needs, and then, according to the function, the design concept will be transformed into a concrete visual representation through interactive prototypes. Then, the visual design of the interface is carried out according to the interactive prototype, and finally, the development of the system is realized by interactive technology, as shown in Figure 10.

After the above system is constructed, the practical effect of the correction model of Chinese dance training movements based on digital feature recognition technology is explored, and the demonstration image shown in Figure 11 is obtained.

On the basis of the above research, the effect evaluation of the correction system of Chinese dance training movements based on digital feature recognition technology in this paper is carried out, and the final results are counted, and the results obtained are shown in Table 1.

From the above analysis, the correction system of Chinese dance training movements based on digital feature recognition technology proposed in this paper has a good effect and can effectively promote the improvement of Chinese dance training effects.

5. Conclusion

The basic skills training of Chinese classical dance has certain standard movements and strict requirements. In the large amount of exercise and long-term training, it is required to maintain correct movements and elegant posture. If the posture of a person's body movement is not correct, not only the movement is not elegant, but, more

importantly, the dancer is prone to injury. Therefore, in the dance teaching of professional colleges, the basic training and teaching of Chinese classical dance is an extremely difficult learning process. This paper combines digital feature recognition technology to correct and analyze Chinese dance training movements and constructs an intelligent auxiliary training system. From the test analysis results, it can be seen that the correction system of Chinese dance training movements based on digital feature recognition technology proposed in this paper has a good effect and can effectively promote the improvement of Chinese dance training effects.

Data Availability

The labeled dataset used to support the findings of this study is available from the corresponding author upon request.

Conflicts of Interest

The authors declare that they have no conflicts of interest.

References

[1] G. Hua, L. Li, and S. Liu, "Multipath affinage stacked—hourglass networks for human pose estimation," *Frontiers of Computer Science*, vol. 14, no. 4, pp. 1–12, 2020.

[2] M. Li, Z. Zhou, and X. Liu, "Multi-person pose estimation using bounding box constraint and LSTM," *IEEE Transactions on Multimedia*, vol. 21, no. 10, pp. 2653–2663, 2019.

[3] S. Liu, Y. Li, and G. Hua, "Human pose estimation in video via structured space learning and halfway temporal evaluation," *IEEE Transactions on Circuits and Systems for Video Technology*, vol. 29, no. 7, pp. 2029–2038, 2018.

[4] W. McNally, A. Wong, and J. McPhee, "Action recognition using deep convolutional neural networks and compressed spatio-temporal pose encodings," *Journal of Computational Vision and Imaging Systems*, vol. 4, no. 1, p. 3, 2018.

[5] D. Mehta, S. Sridhar, O. Sotnychenko et al., "VNect," *ACM Transactions on Graphics*, vol. 36, no. 4, pp. 1–14, 2017.

[6] M. Nasr, H. Ayman, N. Ebrahim, R. Osama, N. Mosaad, and A. Mounir, "Realtime multi-person 2D pose estimation," *International Journal of Advanced Networking and Applications*, vol. 11, no. 6, pp. 4501–4508, 2020.

[7] X. Nie, J. Feng, J. Xing, S. Xiao, and S. Yan, "Hierarchical contextual refinement networks for human pose estimation," *IEEE Transactions on Image Processing*, vol. 28, no. 2, pp. 924–936, 2018.

[8] Y. Nie, J. Lee, S. Yoon, and D. S. Park, "A multi-stage convolution machine with scaling and dilation for human pose estimation," *KSII Transactions on Internet and Information Systems (TIIS)*, vol. 13, no. 6, pp. 3182–3198, 2019.

[9] I. Petrov, V. Shakhuro, and A. Konushin, "Deep probabilistic human pose estimation," *IET Computer Vision*, vol. 12, no. 5, pp. 578–585, 2018.

[10] G. Szűcs and B. Tamás, "Body part extraction and pose estimation method in rowing videos," *Journal of Computing and Information Technology*, vol. 26, no. 1, pp. 29–43, 2018.

[11] N. T. Thành and P. T. Công, "An evaluation of pose estimation in video of traditional martial arts presentation," *Journal of Research and Development on Information and Communication Technology*, vol. 26, no. 2, pp. 114–126, 2019.

[12] J. Xu, K. Tasaka, and M. Yamaguchi, "[Invited paper] fast and accurate whole-body pose estimation in the wild and its applications," *ITE Transactions on Media Technology and Applications*, vol. 9, no. 1, pp. 63–70, 2021.

[13] A. Zarkeshev and C. Csiszár, "Rescue method based on V2X communication and human pose estimation," *Periodica Polytechnica: Civil Engineering*, vol. 63, no. 4, pp. 1139–1146, 2019.

[14] A. Bakshi, D. Sheikh, Y. Ansari, C. Sharma, and H. Naik, "Pose estimate based yoga instructor," *International Journal of Recent Advances in Multidisciplinary Topics*, vol. 2, no. 2, pp. 70–73, 2021.

[15] S. L. Colyer, M. Evans, D. P. Cosker, and A. I. T. Salo, "A review of the evolution of vision-based motion analysis and the integration of advanced computer vision methods towards developing a markerless system," *Sports medicine - open*, vol. 4, no. 1, pp. 24–15, 2018.

[16] I. Sárándi, T. Linder, K. O. Arras, and B. Leibe, "Metrabs: metric-scale truncation-robust heatmaps for absolute 3d human pose estimation," *IEEE Transactions on Biometrics, Behavior, and Identity Science*, vol. 3, no. 1, pp. 16–30, 2020.

[17] A. Azhand, S. Rabe, S. Müller, I. Sattler, and A. Heimann-Steinert, "Algorithm based on one monocular video delivers highly valid and reliable gait parameters," *Scientific Reports*, vol. 11, no. 1, p. 10, Article ID 14065, 2021.

[18] J. Xu and K. Tasaka, "[Papers] keep your eye on the ball: detection of kicking motions in multi-view 4K soccer videos," *ITE Transactions on Media Technology and Applications*, vol. 8, no. 2, pp. 81–88, 2020.